LHCb Note 2007-041
PHYSICS

$\gamma + \phi_s$ sensitivity studies from combined $B_s^0 \to D_s^- \pi^+$ and $B_s^0 \to D_s^\mp K^\pm$ samples at LHCb

S. Cohen, M. Merk, E. Rodrigues

shirit.cohen@cern.ch

marcel.merk@nikhef.nl

eduardo.rodrigues@cern.ch

NIKHEF, Amsterdam, The Netherlands

July 2007

Abstract

At the LHCb experiment the decay channels $B_s^0 \to D_s^- \pi^+$ and $B_s^0 \to D_s^\mp K^\pm$ will be used to determine the physics parameters Δm_s and $\gamma + \phi_s$. By performing toy Monte Carlo simulation studies, using information from a full GEANT LHCb simulation, we expect statistical uncertainties of $\sigma(\Delta m_s) = 0.007\,\mathrm{ps}^{-1}$ and $\sigma(\gamma + \phi_s) = 10.3^\circ$ for an integrated luminosity of $2\,\mathrm{fb}^{-1}$.

Contents

1 Introduction

The decay channels $B_s^0 \to D_s^- \pi^+$ and $B_s^0 \to D_s^\mp K^\pm$ and their charge conjugate modes[1] will be used in the LHCb experiment to extract Δm_s, the $B_s^0 - \bar{B}_s^0$ mass difference (and oscillation frequency) and the CP angle $\gamma + \phi_s$. The two channels have several physics quantities in common, and identical topologies. For this reason both modes are analysed simultaneously in a combined fit.

This note describes toy Monte Carlo (MC) sensitivity studies that were performed using the RooFit software package [1]. Experimental parameters obtained from a full LHCb offline selection study [2] were used in the toy MC (*e.g.* event yields, background level, reconstructed B_s^0 mass distribution, etc.).

In section 2 the B_s^0 decay equations are given and the method to extract the relevant physics parameters is shown. In section 3 the simulation program is presented and the likelihood function explained. The results are finally reported in section 4.

2 Theory

2.1 $B_s^0 \to D_s^- \pi^+$ and $B_s^0 \to D_s^\mp K^\pm$ decay channels

The relations between the B_s^0-meson mass eigenstates, $|B_{H,L}\rangle$, and their flavour eigenstates, $|B_s^0\rangle$ and $|\bar{B}_s^0\rangle$, can be expressed in terms of linear coefficients p and q:

$$|B_{H,L}\rangle = p|B_s^0\rangle \mp q|\bar{B}_s^0\rangle \quad . \tag{1}$$

We define the differences in mass and decay rate as:

$$\Delta m_s = m_H - m_L \quad , \quad \Delta\Gamma_s = \Gamma_H - \Gamma_L \quad . \tag{2}$$

The average mass and decay rate are defined by:

$$m_s = \frac{m_H + m_L}{2} \quad , \quad \Gamma_s = \frac{\Gamma_H + \Gamma_L}{2} \quad . \tag{3}$$

The decay rate at time t of an originally produced $|B_s^0\rangle$ to a final state f is given by:

$$\Gamma_{B_s^0 \to f}(t) = |\langle f|T|B_s^0(t)\rangle|^2 \quad , \tag{4}$$

where T is the transition matrix element. Similar expressions exist for $\bar{B}_s^0$ and $\bar{f}$.

[1] Unless specified otherwise, charge conjugate modes are assumed throughout this paper.

The time evolution of the flavour eigenstates $|B_s^0\rangle$ and $|\bar{B}_s^0\rangle$ are then given by the four decay equations

$$\Gamma_{B_s^0\to f}(t) = |A_f|^2(1+|\lambda_f|^2)\frac{e^{-\Gamma_s t}}{2}\cdot \left(\cosh\frac{\Delta\Gamma_s t}{2} + D_f \sinh\frac{\Delta\Gamma_s t}{2} + C_f\cos\Delta m_s t - S_f \sin\Delta m_s t\right) \quad , \tag{5}$$

$$\Gamma_{\bar{B}_s^0\to f}(t) = |A_f|^2\left|\frac{p}{q}\right|^2(1+|\lambda_f|^2)\frac{e^{-\Gamma_s t}}{2}\cdot \left(\cosh\frac{\Delta\Gamma_s t}{2} + D_f \sinh\frac{\Delta\Gamma_s t}{2} - C_f\cos\Delta m_s t + S_f \sin\Delta m_s t\right) \quad , \tag{6}$$

$$\Gamma_{\bar{B}_s^0\to \bar{f}}(t) = |\bar{A}_{\bar{f}}|^2(1+|\bar{\lambda}_{\bar{f}}|^2)\frac{e^{-\Gamma_s t}}{2}\cdot \left(\cosh\frac{\Delta\Gamma_s t}{2} + D_{\bar{f}} \sinh\frac{\Delta\Gamma_s t}{2} + C_{\bar{f}}\cos\Delta m_s t - S_{\bar{f}} \sin\Delta m_s t\right) \quad , \tag{7}$$

$$\Gamma_{B_s^0\to \bar{f}}(t) = |\bar{A}_{\bar{f}}|^2\left|\frac{q}{p}\right|^2(1+|\bar{\lambda}_{\bar{f}}|^2)\frac{e^{-\Gamma_s t}}{2}\cdot \left(\cosh\frac{\Delta\Gamma_s t}{2} + D_{\bar{f}} \sinh\frac{\Delta\Gamma_s t}{2} - C_{\bar{f}}\cos\Delta m_s t + S_{\bar{f}} \sin\Delta m_s t\right) \quad , \tag{8}$$

where

$$D_f = \frac{2Re\lambda_f}{1+|\lambda_f|^2} \quad , \quad C_f = \frac{1-|\lambda_f|^2}{1+|\lambda_f|^2} \quad , \quad S_f = \frac{2Im\lambda_f}{1+|\lambda_f|^2} \quad ,$$
$$D_{\bar{f}} = \frac{2Re\bar{\lambda}_{\bar{f}}}{1+|\bar{\lambda}_{\bar{f}}|^2} \quad , \quad C_{\bar{f}} = \frac{1-|\bar{\lambda}_{\bar{f}}|^2}{1+|\bar{\lambda}_{\bar{f}}|^2} \quad , \quad S_{\bar{f}} = \frac{2Im\bar{\lambda}_{\bar{f}}}{1+|\bar{\lambda}_{\bar{f}}|^2} \quad . \tag{9}$$

A_f and $\bar{A}_{\bar{f}}$ are the decay amplitudes (*e.g.* $A_f = \langle f|T|B_s^0\rangle$) and

$$\lambda_f \equiv \frac{q}{p}\frac{\bar{A}_f}{A_f} \quad , \quad \bar{\lambda}_{\bar{f}} \equiv \frac{p}{q}\frac{A_{\bar{f}}}{\bar{A}_{\bar{f}}} \quad .$$

In this analysis we are interested in the decays $B_s^0 \to D_s^-\pi^+$ and $B_s^0 \to D_s^\mp K^\pm$. The Feynman diagrams for both decays are given in Fig. 1.

For the $B_s^0 \to D_s^-\pi^+$ channel only one tree diagram exists such that a B_s^0 can only decay instantaneously into $D_s^-\pi^+$ final state, while the decay into $D_s^+\pi^-$ can only occur after mixing. The decay $B_s^0 \to D_s^-\pi^+$ is therefore flavour specific, leading to $A_{\bar{f}} = \bar{A}_f = 0$, thus $\lambda_f = \bar{\lambda}_{\bar{f}} = 0$. This in turn leads to the parameters $D_f = S_f = 0$ and $C_f = 1$.

The parameter Δm_s can be obtained from the $B_s^0 \to D_s^-\pi^+$ channel via the flavour asymmetry, defined as

$$A^{flav} = \frac{\Gamma_{\bar{B}_s^0\to f} - \Gamma_{B_s^0\to f}}{\Gamma_{\bar{B}_s^0\to f} + \Gamma_{B_s^0\to f}} = -D\cdot\frac{cos(\Delta m_s t)}{cosh(\frac{\Delta\Gamma_s t}{2})} \quad , \tag{10}$$

with the assumption $\left|\frac{p}{q}\right| = 1$. D is a dilution factor with contributions from wrong B_s^0 flavour tagging ($1-2\omega$, where ω is the wrong tag fraction) and experimental decay time

Figure 1: Feynman diagrams for $B_s^0 \to D_s^- \pi^+$ (top), $B_s^0 \to D_s^- K^+$ tree diagram $T1$ (bottom left) and $\bar{B}_s^0 \to D_s^- K^+$ tree diagram $T2$ (bottom right). The sub-process $T1$ has a larger magnitude than $T2$ due to the different coupling constants.

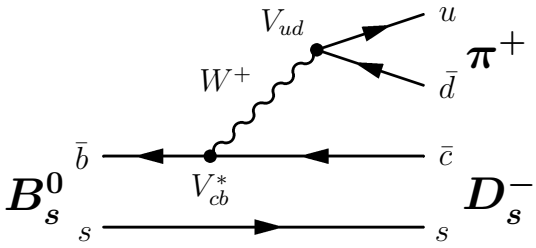

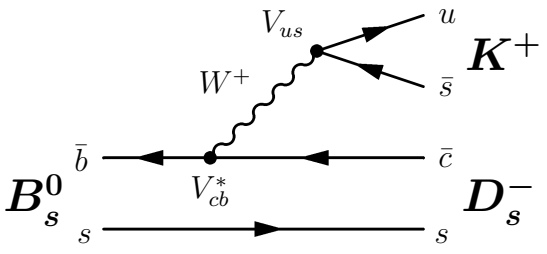

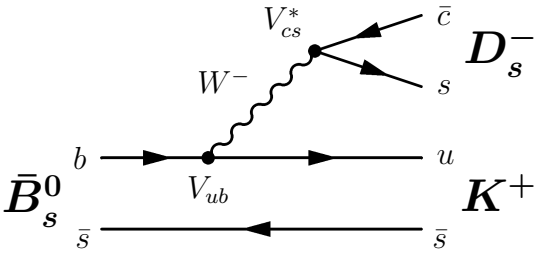

resolutions. Using A^{flav} one can obtain Δm_s, ω and optionally $\Delta\Gamma_s$ from the decay rates $\Gamma_{B_s^0 \to f}$ and $\Gamma_{\bar{B}_s^0 \to f}$, and similarly from $\Gamma_{B_s^0 \to \bar{f}}$ and $\Gamma_{\bar{B}_s^0 \to \bar{f}}$.

As kaons contain an s quark, two tree diagrams for instantaneous decay exist for the $B_s^0 \to D_s^{\mp} K^{\pm}$ channels (see Fig.1). A B_s^0 meson, as well as a $\bar{B}_s^0$, can decay directly (without oscillations) to $D_s^- K^+$ or to $D_s^+ K^-$, therefore this decay channel is not flavour specific. Due to the different coupling constants the two tree diagrams T_1 and T_2 have different magnitudes. The process $B_s^0 \to D_s^+ K^-$ (tree diagram T_2) is "Cabibbo suppressed" due to flavour change from the third to first quark generation described by V_{ub}.

As each decay is dominated by a single diagram, for $B_s^0 \to D_s^{\mp} K^{\pm}$ we have $|A_f| = |\bar{A}_{\bar{f}}|$ and $|A_{\bar{f}}| = |\bar{A}_f|$. Using the assumption $\left|\frac{p}{q}\right| = 1$ this gives $|\lambda_f| = |\bar{\lambda}_{\bar{f}}|$. As a B_s^0 and a $\bar{B}_s^0$ can both decay instantaneously as $D_s^- K^+$ there is an interference between the B_s^0 decays where the B_s^0 has or has not oscillated. Taking into account the quark processes involved, the interference affects are expected to be large. The terms λ_f and $\bar{\lambda}_{\bar{f}}$ are then calculated by:

$$\lambda_{D_s^- K^+} = \left(\frac{q}{p}\right) \frac{\bar{A}_{D_s^- K^+}}{A_{D_s^- K^+}} = \left(\frac{V_{tb}^* V_{ts}}{V_{tb} V_{ts}^*}\right) \left(\frac{V_{ub} V_{cs}^*}{V_{cb}^* V_{us}}\right) \left|\frac{A_2}{A_1}\right| e^{i\Delta_{T1/T2}} = |\lambda_{D_s^- K^+}| e^{i(\Delta_{T1/T2} - (\gamma + \phi_s))} \quad ,$$

$$\bar{\lambda}_{D_s^+K^-} = \Big(\frac{p}{q}\Big)\frac{A_{D_s^+K^-}}{\bar{A}_{D_s^+K^-}} = \Big(\frac{V_{tb}V_{ts}^*}{V_{tb}^*V_{ts}}\Big)\Big(\frac{V_{ub}^*V_{cs}}{V_{cb}V_{us}^*}\Big)\Big|\frac{A_2}{A_1}\Big|e^{i\Delta_{T1/T2}} = |\lambda_{D_s^-K^+}|e^{i(\Delta_{T1/T2}+(\gamma+\phi_s))} \quad , (11)$$

where $|A_2/A_1|$ is the ratio of the hadronic amplitudes, $\Delta_{T1/T2}$ is the strong phase difference between $T1$ and $T2$, and $\gamma+\phi_s$ is the weak phase. The strong and the weak phases can be extracted using the relations:

$$\gamma+\phi_s = \frac{1}{2}[arg(\bar{\lambda}_{\bar{f}}) - arg(\lambda_f)] \quad ,$$

$$\Delta_{T1/T2} = \frac{1}{2}[arg(\bar{\lambda}_{\bar{f}}) + arg(\lambda_f)] \quad . \qquad (12)$$

The small ϕ_s angle originates from B_s^0 mixing and can be measured directly, for example using the decay $B_s^0 \to J/\psi\phi$ [3]. The expected (combined) sensitivity from several B-decays is 0.021 rad for 2 fb^{-1} of data [4]. Combining such measurement with the presented method of extracting $\gamma+\phi_s$ from $B_s^0 \to D_s^{\mp}K^{\pm}$ is a theoretically clean way to measure the CKM matrix angle γ.

For the extraction of $\gamma+\phi_s$ the values for Δm_s, $\Delta\Gamma_s$ and ω are needed. These can be determined from the $B_s^0 \to D_s^-\pi^+$ channel, as shown above. In order to get the best resolutions on the different fit parameters and to take correlations into account, a simultaneous fit is made on both $B_s^0 \to D_s^-\pi^+$ and $B_s^0 \to D_s^{\mp}K^{\pm}$ decay rates. This is justified since the two decay channels are topologically similar, and the event selection is the same except for the requirements of particle identification (PID) on the bachelor particle (pion or kaon) [2]. The wrong tag fraction value, ω, is assumed to be equal for both channels, as was confirmed in a LHCb tagging performance study [5].

3 Simulation and Likelihood function minimization

3.1 RooFit simulation

A toy Monte Carlo study was performed in order to study the sensitivity for Δm_s and $\gamma+\phi_s$. The RooFit program was used for modeling probability distribution functions (PDFs) such as the decay rates, the reconstructed B_s^0 mass distribution, etc. Event distributions were defined in time and mass dimensions. Events were generated according to the appropriate PDFs and fitted back with the same PDFs. We have used a RooFit built-in interface which connects RooFit to the MINUIT minimization package [6]. The MIGRAD minimization method of MINUIT was used for all studies presented in this note.

[2] The bachelor particle refers to the final state particle that does not originate from the D_s

3.2 Input parameters for the simulation

The generation of PDFs which match as closely as possible the expected LHCb data distributions needs correct assumptions on the physics and detector parameters. The full set of parameters that were used for the toy MC study are listed below.
The physics parameters used in the simulation are:

- B_s^0 meson mass $m_{B_s^0} = 5367.5\,\mathrm{MeV/c^2}$ and B_s^0 lifetime $\tau = 1.46$ ps ;
- B_s^0 oscillation frequency $\Delta m_s = 17.5\ \mathrm{ps}^{-1}$, $\Delta\Gamma_s/\Gamma_s = 0.1$;
- $|\lambda_f| = 0.37$, weak phase $\gamma + \phi_s = 60^\circ$ and strong phase $\Delta_{T1/T2} = 0^\circ$ unless specified otherwise .

The LHCb experiment-related parameters that are used in the toy MC program are the result of a full offline selection study that was performed, using the official LHCb simulated data (the so-called DC04 data sample) and software packages. A full report of the offline selection study is found in [2]. The experiment-related parameters that are used in the simulation are:

- Event yields for an integrated luminosity of $2\,\mathrm{fb}^{-1}$: 140 k events ($B_s^0 \to D_s^-\pi^+$) and 6.2 k events ($B_s^0 \to D_s^\mp K^\pm$). We define $2\,\mathrm{fb}^{-1}$ as one year of data taking.
- B_s^0 mistag fraction $\omega = 0.328$ and tagging efficiency $\varepsilon_{tag} = 0.5812$ ($B_s^0 \to D_s^-\pi^+$ and $B_s^0 \to D_s^\mp K^\pm$).
- Background-to-signal ratio: $B/S = 0.2$ ($B_s^0 \to D_s^-\pi^+$), and $B/S = 0.7$ ($B_s^0 \to D_s^\mp K^\pm$).
- Reconstructed B_s^0 mass resolution $\sigma(m_{B_s^0}) = 14\,\mathrm{MeV/c^2}$. The reconstructed B_s^0 distribution plots from the offline selection study are given in Fig. 2.
- Estimation of the B_s^0 reconstructed decay time (proper time) error $\Delta\tau_{rec}$. The distribution of per-event proper time errors from the offline selection study and its pull distribution are given in Fig. 3. The distribution has a mean value of 33fs and a most probable value of 30fs. The parametrization that was fitted to the histogram and was used to build a proper time error PDF in the RooFit simulation is reported in Tab. 1 and plotted in Fig. 3.
- Acceptance function, defined as selection efficiency versus the proper time. The acceptance obtained from the DC04 offline selection study is shown in Fig. 4. The

parametrization that was found for the acceptance distribution and was used to simulate it within the RooFit study (also reported in the figure) is given by:

$$\begin{aligned} A(\tau_{rec} < 0\,\mathrm{ps}) &= 0 \quad , \\ A(0\,\mathrm{ps} < \tau_{\mathrm{rec}} < 15\,\mathrm{ps}) &= \frac{(0.98 \cdot \tau_{rec})^{2.11}}{1 + (0.98 \cdot \tau_{rec})^{2.11}} \cdot (1 - 0.066 \cdot \tau_{rec}) \quad , \\ A(15\,\mathrm{ps} < \tau_{\mathrm{rec}}) &= 0 \quad . \end{aligned}$$

The time dependence of the acceptance function is assumed to be identical for $D_s\pi$ and D_sK events.

Proper time error distribution parametrization	
$\Delta\tau_{rec}$ value (ps)	Distribution ($\Delta\tau_{rec}$)
$\Delta\tau_{rec} < 0.005$	0
$0.005 < \Delta\tau_{rec} < 0.03$	13592 * Landau($\Delta\tau_{rec}$, 0.029, 0.0062)
$0.03 < \Delta\tau_{rec} < 0.1$	21331 * Gaussian($\Delta\tau_{rec}$, -0.015, 0.0217)
$0.1 < \Delta\tau_{rec}$	0

Table 1: Proper time error distribution parametrization. For both the Landau and the Gaussian distributions the input parameters stand for (x, mean, sigma).

Due to low statistics, the offline selection study reports only upper limits on the B/S ratios for combinatorial and specific background. For this study we chose to use the central value of the specific background (which gave the higher B/S ratio between the two), yielding the numbers reported above. A summary of the input parameters that are used in the toy MC RooFit simulation is given in Tab. 2.

3.3 Likelihood function description

The sensitivity studies reported in this note follow previous studies that were performed involving these decay channels [7, 8]. For the toy MC study the following approach was implemented. Events are generated according to the toy MC model of the $B_s^0 \to D_s^-\pi^+$ and $B_s^0 \to D_s^\mp K^\pm$ decays at the LHCb experiment. Data are collected using the nominal values given in section 3.2 and with a certain configuration (the different configurations are explained in section 4). An event is described by a generated reconstructed proper time (τ_{rec}) and a generated B_s^0 reconstructed mass (m_{rec}). An experimental uncertainty on the proper time ($\Delta\tau_{rec}$) is assigned to each event.

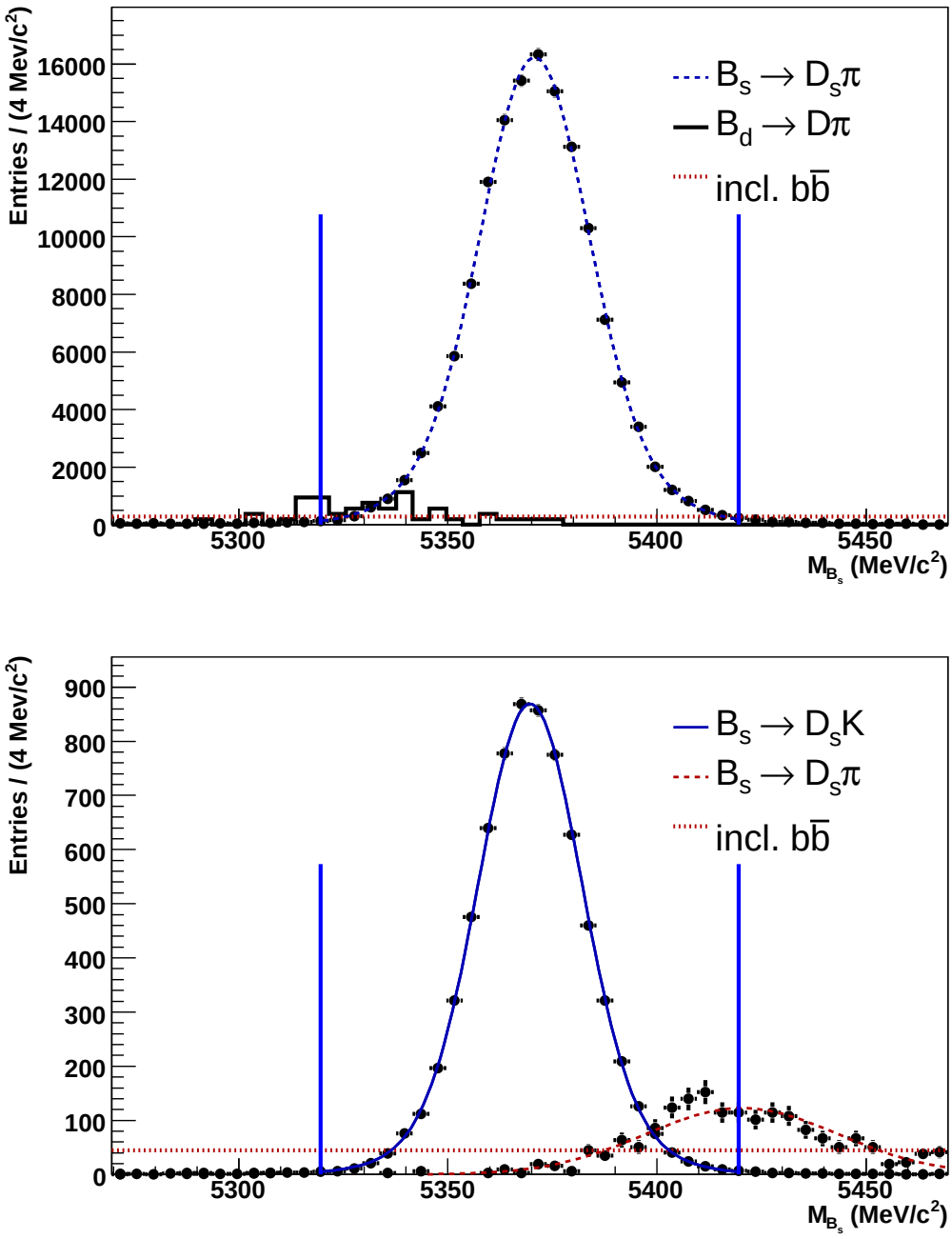

Figure 2: Reconstructed B_s^0 mass distribution from the full offline selection study, including signal and main background contributions (reported after trigger). Histograms are normalized for one year of data taking ($2\,\text{fb}^{-1}$). Top: reconstructed B_s^0 mass from $B_s^0 \to D_s^- \pi^+$ decays. Bottom: reconstructed B_s^0 mass from $B_s^0 \to D_s^\mp K^\pm$ decays. The small lower peak on the right is due to misidentified $B_s^0 \to D_s^- \pi^+$ decays. Plots taken from [2].

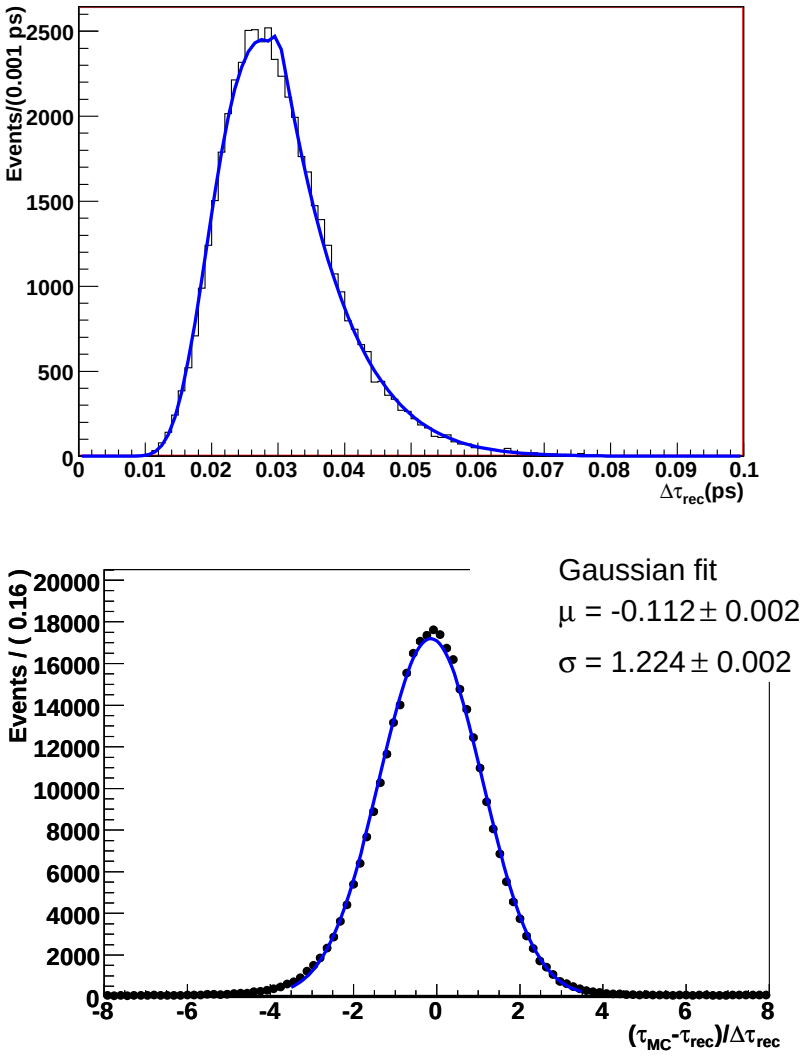

Figure 3: Proper time error plots (no trigger applied). Top: proper time error estimate distribution from full LHCb selection study. The fitted curve is the PDF as it is used in the sensitivity studies. Bottom: pull distribution of the proper time error, i.e. $(\tau_{rec} - \tau_{true})/\Delta\tau_{rec}$ fitted with a Gaussian distribution. The sigma of the pull distribution shows that the errors are underestimated. The histograms are taken from [2].

Toy MC input parameters	
Parameter	Input value
$\sigma(m_{B_s^0})$ (MeV/c^2)	14
$\Delta\Gamma_s/\Gamma_s$	0.1
Δm_s (ps^{-1})	17.5
mistag fraction ω	0.328
tagging efficiency ε_{tag}	0.5812
$\lvert\lambda_f\rvert$	0.37
$\gamma + \phi_s$ ($^\circ$)	60
$\Delta_{T1/T2}$ ($^\circ$)	0
$B_s^0 \to D_s^- \pi^+$ event yield (1 year)	140 k
$B_s^0 \to D_s^\mp K^\pm$ event yield (1 year)	6.2 k
$B_s^0 \to D_s^- \pi^+$ B/S ratio	0.2
$B_s^0 \to D_s^\mp K^\pm$ B/S ratio	0.7

Table 2: Input parameter values for the toy MC simulation program.

The per-event proper time error distribution and its pull distribution are shown in Fig. 3. The pull shows that the proper time errors from the full MC simulation are underestimated and suffer from a significant bias. In the toy MC we correct for the underestimated errors by re-scaling the errors with a scale factor[3]. The bias was not simulated in the toy MC. Background events are generated with a lifetime that is half the B_s^0 meson lifetime in order to simulate wrong associations of tracks originating from the primary vertex to the reconstructed B_s^0 decay. The events are used to maximize a likelihood function ($\mathcal{L}$) which is given by:

$$\mathcal{L}_{B_s^0 \to f}(\vec{\alpha}, \vec{\beta}) = \prod_i^{B_s \to D_s \pi} \mathrm{Prob}(\tau_{rec}, m_{rec}, \Delta\tau_{rec} | \vec{\alpha}, S_{sig}, S_{bg}, \omega) \times \prod_i^{B_s \to D_s K} \mathrm{Prob}(\tau_{rec}, m_{rec}, \Delta\tau_{rec} | \vec{\beta}, S_{sig}, S_{bg}, \omega) \quad , \tag{13}$$

with $\vec{\alpha} = (\Gamma_s, \Delta m_s, \Delta\Gamma_s)$ and $\vec{\beta} = (\lambda_f, \bar{\lambda}_{\bar{f}}, \Gamma_s, \Delta m_s, \Delta\Gamma_s)$ the vectors of physics parameters used for the event generation.

[3]We scale the errors with a factor 1.175, which at the time was the reported value for the pull sigma. With a new Gaussian fit the pull sigma was later updated to 1.224.

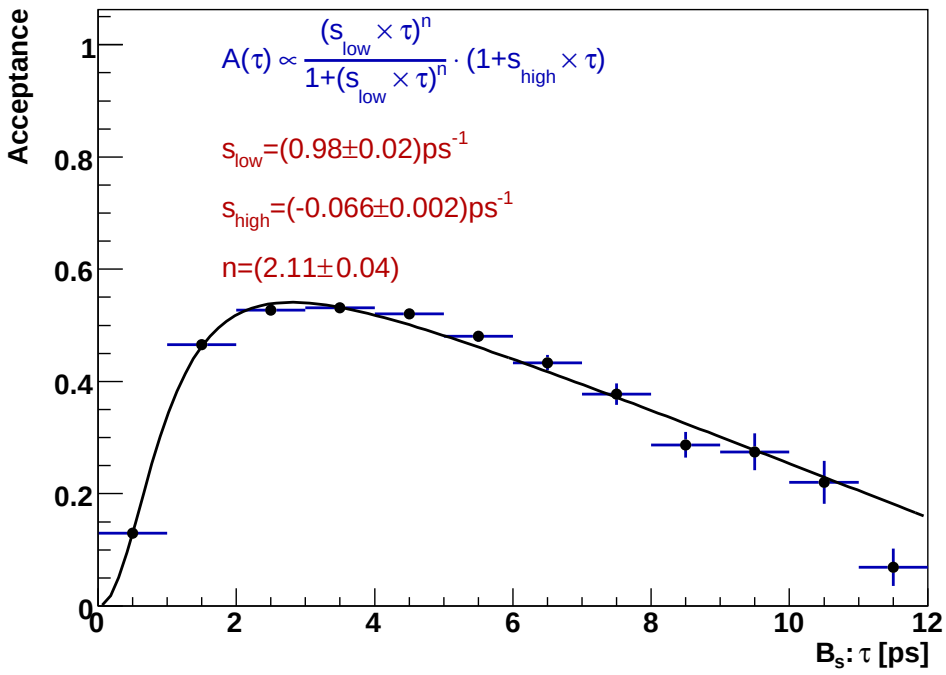

Figure 4: Acceptance function versus the proper time from the full offline selection study (DC04 data) and the parametrization that was fitted to it. The acceptance is reported after trigger. Plot taken from [2].

The PDFs are given by:

$$\begin{aligned}
&\mathrm{Prob}(\tau_{rec}, m_{rec}, \Delta\tau_{rec}|\vec{\alpha}, S_{sig}, S_{bg}, \omega) = \\
&\int_0^\infty \Big\{ \Big[(1-f_{bg}) M_{sig}(m_{rec}) \Gamma_{sig}(t|\vec{\alpha},\omega)\Big] \cdot A(t) \cdot G_{sig}(t-\tau_{rec}, \Delta\tau_{rec}, S_{sig}) \\
&+ \Big[f_{bg} M_{bg}(m_{rec}) \Gamma_{bg}(t)\Big] \cdot A(t) \cdot G_{bg}(t-\tau_{rec}, \Delta\tau_{rec}, S_{bg})\Big\} \cdot dt \quad , \qquad (14)
\end{aligned}$$

with the different distributions defined by:

- Signal decay rate: $\Gamma_{sig}(t|\vec{\alpha},\omega) = (1-\omega)\Gamma_{B_s^0 \to f} + \omega\Gamma_{\bar{B}_s^0 \to f}$ with ω the wrong tag fraction.
- Background decay rate: $\Gamma_{bg}(t) = 2\Gamma_s e^{-2t\Gamma_s}$.
- Signal reconstructed B_s^0 mass: $M_{sig}(m_{rec}) = \frac{1}{(\sigma_{m_{B_s^0}})\sqrt{2\pi}} e^{-(m_{rec}-m_{B_s^0})^2/2(\sigma_{m_{B_s^0}})^2}$, with $\sigma_{m_{B_s^0}} = 14\,\mathrm{MeV}$ and $m_{B_s^0}$ the B_s^0 meson mass.
- Background reconstructed B_s^0 mass: $M_{bg}(m_{rec}) =$ constant.

- Acceptance: $A(t)$ is the proper time dependent acceptance function as determined from the full LHCb simulation. (Fig. 4).

- Signal decay time smearing with a per-event error:

$$G_{sig}(t-\tau_{rec},\Delta\tau_{rec},S_{sig}) = \frac{1}{(\Delta\tau_{rec}\cdot S_{sig})\sqrt{2\pi}} e^{-(\tau_{rec}-t)^2/2(S_{sig}\cdot\Delta\tau_{rec})^2} \quad .$$

  For each event $\Delta\tau_{rec}$ is sampled from the per-event proper time error distribution obtained from the full LHCb simulation (Fig. 3). The decay time is then smeared with a Gaussian with a width of $\Delta\tau_{rec}\cdot S_{sig}$, where S_{sig} is a scale factor applied to signal events.

- Background decay time smearing with a per-event error:

$$G_{bg}(t-\tau_{rec},\Delta\tau_{rec},S_{bg}) = \frac{1}{(\Delta\tau_{rec}\cdot S_{bg})\sqrt{2\pi}} e^{-(\tau_{rec}-t)^2/2(S_{bg}\cdot\Delta\tau_{rec})^2} \quad .$$

  Similar to the smearing of the signal decay time explained above but with a background scale factor, S_{bg}.

Identical definitions hold for $\mathrm{Prob}(\tau_{rec}, m_{rec}, \Delta\tau_{rec}|\vec{\beta}, S_{sig}, S_{bg}, \omega)$. The total likelihood is given by:

$$\mathcal{L}(\vec{\alpha},\vec{\beta}) = \mathcal{L}_{B_s^0\to f}(\vec{\alpha},\vec{\beta})\cdot\mathcal{L}_{\bar{B}_s^0\to f}(\vec{\alpha},\vec{\beta})\cdot\mathcal{L}_{B_s^0\to \bar{f}}(\vec{\alpha},\vec{\beta})\cdot\mathcal{L}_{\bar{B}_s^0\to \bar{f}}(\vec{\alpha},\vec{\beta}) \quad . \tag{15}$$

The events are weighted according to the fraction of events with that mass that are selected in the offline event selection. This fraction follows from the reconstructed mass distribution as determined in the event selection with the full LHCb simulation (Fig. 2). Two resolution scale factors for signal and background, S_{sig} and S_{bg}, are introduced in the likelihood and are multiplied with $\Delta\tau_{rec}$. If a resolution scale factor is a floating parameter in the likelihood maximization then its fitted value may not be consistent with its input value, indicating an error in the determination of the uncertainty on the proper time.

The time dependent acceptance function is shown in Fig. 4. The full LHCb simulation selection efficiency was obtained from the combined samples ($B_s^0 \to D_s^-\pi^+$ and $B_s^0 \to D_s^\mp K^\pm$), as the selections of the two differ only in the bachelor particle identification.

The combined likelihood for $B_s^0 \to D_s^-\pi^+$ and $B_s^0 \to D_s^\mp K^\pm$ is simultaneously maximized; the floating parameters in the fit are: $|\lambda_f|(=|\bar{\lambda}_{\bar{f}}|)$, $arg(\lambda_f)$, $arg(\bar{\lambda}_{\bar{f}})$, ω and Δm_s. The values for the weak and the strong phases ($\gamma+\phi_s$ and $\Delta_{T1/T2}$, respectively) follow from Eq. 12.

4 Results

4.1 Simulated events

In Fig. 5 we present an example of the RooFit distributions of the $B_s^0 \to D_s^- \pi^+$ and $\bar{B}_s^0 \to D_s^- \pi^+$ channels. The plots show the distribution of simulated events and a curve representing the maximized likelihood function projected onto the proper time axis, representing five years of data taking (10 fb^{-1}). The observed distributions originate from the B_s^0 decay equations (Eqs. 5-8) with the appropriate physics parameters and including experimental resolution effects. The B_s^0 oscillations are damped in amplitude due to mistagged events and smeared due to the detector resolution on the reconstructed proper time. The effect of the acceptance function is seen for proper times smaller than 2 ps. Similar plots for the two $B_s^0 \to D_s^{\mp} K^{\pm}$ and two $\bar{B}_s^0 \to D_s^{\pm} K^{\mp}$ decay flavour distributions are given in Fig. 6. One can see that the statistical fluctuations in the $B_s^0 \to D_s^{\mp} K^{\pm}$ channel are larger than those in the $B_s^0 \to D_s^- \pi^+$ channel, as expected from the order of magnitude difference in sample sizes. Figure 7 shows distributions for the invariant mass and the experimental uncertainty in the proper time, for 10 fb^{-1} of data taking. The curves are the corresponding projections of the multidimensional PDF.

Sensitivity results from $B_s^0 \to D_s^- \pi^+$ and $B_s^0 \to D_s^{\mp} K^{\pm}$					
	$\Delta m_s\,(\mathrm{ps}^{-1})$	ω	$\lvert\lambda_f\rvert$	$\gamma + \phi_s\,(^\circ)$	$\Delta_{T1/T2}\,(^\circ)$
Input value	17.5	0.328	0.37	60	0
Fitted value	17.5	0.3279	0.373	60.3	0.5
σ (5y)	0.003	0.0013	0.029 ± 0.0011	5.7 ± 0.2	5.4 ± 0.2
σ (1y)	0.007	0.0030	0.066	12.7	12.1

Table 3: Sensitivity results from $B_s^0 \to D_s^- \pi^+$ and $B_s^0 \to D_s^{\mp} K^{\pm}$ tagged event samples.

4.2 Sensitivity studies results

For obtaining the expected resolutions on Δm_s, $\gamma + \phi_s$ and $\Delta_{T1/T2}$ we performed 400 "experiments" with each containing 5 years of tagged data at LHCb (10 fb^{-1}). A Gaussian distribution was fitted to the collection of the 400 fitted values for each fitted parameter. The mean and the standard deviation (sigma) of the fitted Gaussians are reported as the fitted value and the resolution for 10 fb^{-1} in Tab. 3. The resolutions are also scaled for 1 year of data taking and reported in the table. The pull distribution for each of the fitted parameters was plotted and found to be consistent with having no bias and a width of 1.

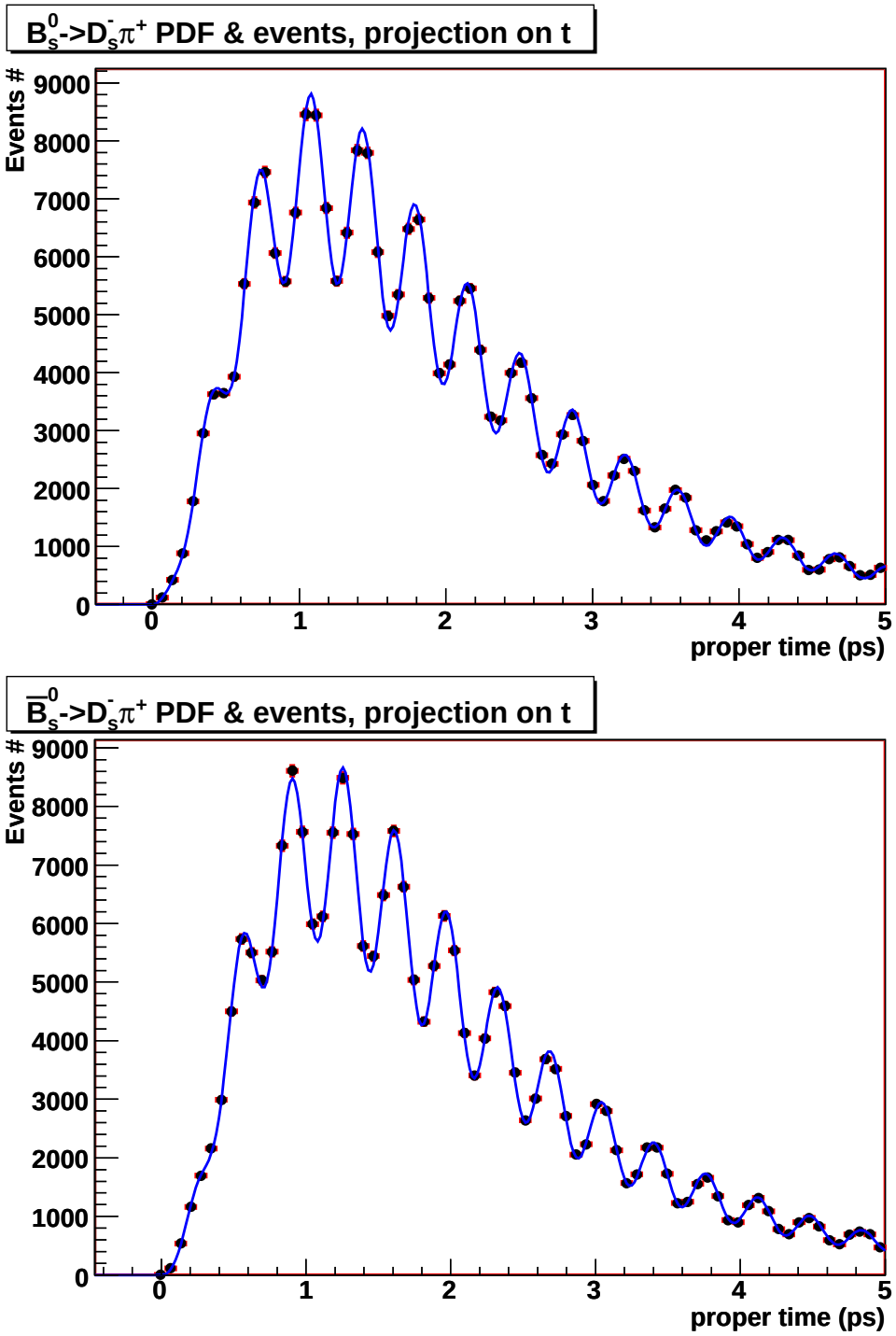

Figure 5: RooFit simulated proper time distributions for $B_s^0 \to D_s^- \pi^+$ (top) and $\bar{B}_s^0 \to D_s^- \pi^+$ (bottom). The simulated events and the maximized likelihood curve are projected onto the proper time axis, representing 10 fb^{-1} of data. The error bars on the data points are of the same size as the markers.

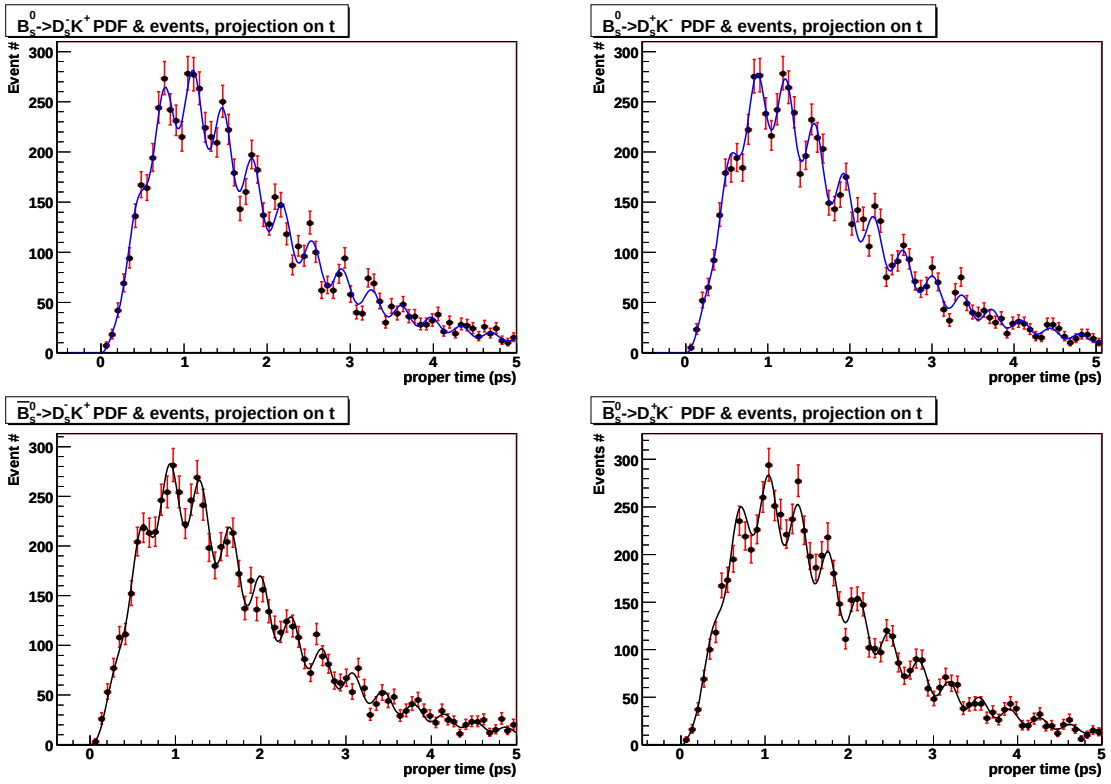

Figure 6: RooFit simulated proper time distributions for $B_s^0 \to D_s^- K^+$ (top left), $B_s^0 \to D_s^+ K^-$ (top right), $\bar{B}_s^0 \to D_s^- K^+$ (bottom left) and $\bar{B}_s^0 \to D_s^+ K^-$ (bottom right). The simulated events and the maximized likelihood curve are projected onto the proper time axis, representing 10 fb^{-1} of data.

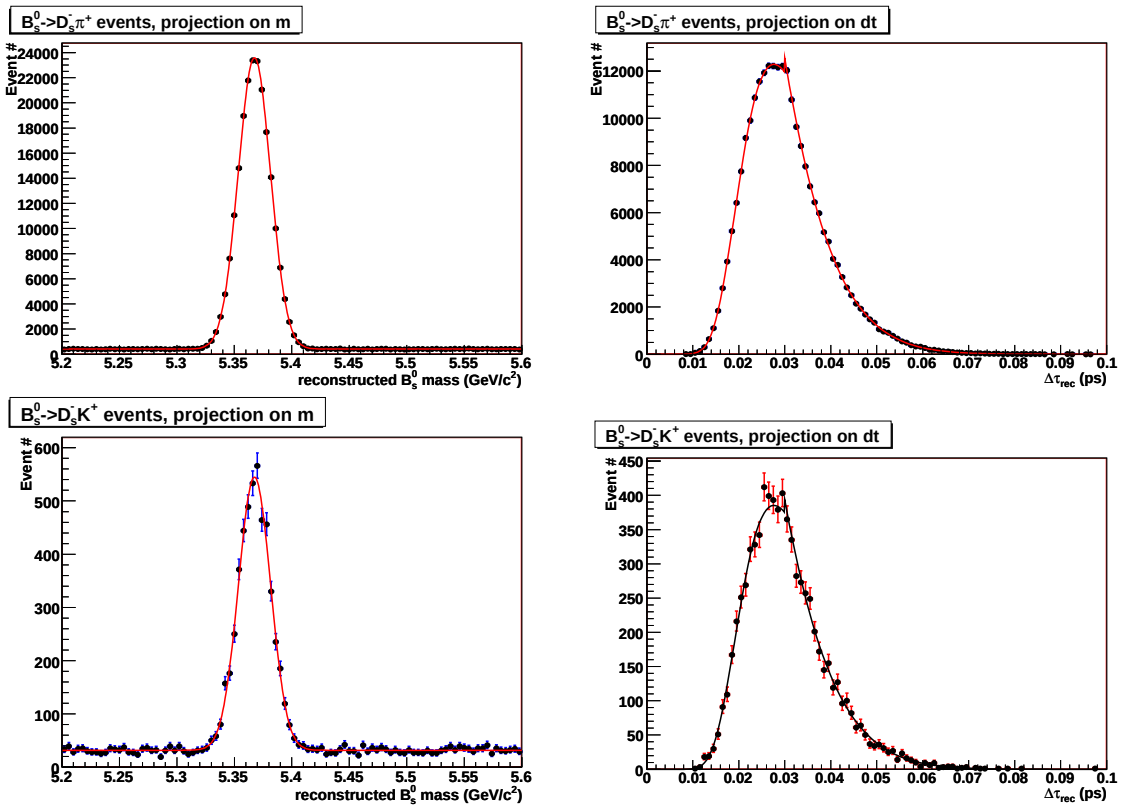

Figure 7: Roofit simulated reconstructed B_s^0 mass and proper time error distributions for $B_s^0 \to D_s^- \pi^+$ (top) and $B_s^0 \to D_s^- K^+$ (bottom). The distributions represent 10 fb^{-1} of data. All the parameters that are connected to the reconstructed B_s^0 mass and the proper time error distributions have been fixed parameters in the likelihood maximization.

We note a resolution of $\sigma(\Delta m_s) = 0.007\,\mathrm{ps}^{-1}$, a determination of ω at a level of $\sim 1\%$, and a resolution of $\sigma(\gamma + \phi_s) = 12.7^\circ$ after one year of LHCb data using solely tagged events.

4.3 Results when including $B_s^0 \to D_s^\mp K^\pm$ untagged events

For the $B_s^0 \to D_s^\mp K^\pm$ case, the untagged events hold additional information on the phases and can be added to the analysis in order to obtain increased sensitivity. Assuming as before $\left|\frac{p}{q}\right| = 1$, the decay rate equations (Eqs. 5-8) are reduced in the untagged events case to two equations:

$$\Gamma_{B_s^0/\bar{B}_s^0 \to f}(t) = 2 \cdot |A_f|^2 (1 + |\lambda_f|^2) \frac{e^{-\Gamma_s t}}{2} \cdot \left(\cosh \frac{\Delta\Gamma_s t}{2} + D_f \sinh \frac{\Delta\Gamma_s t}{2} \right) \quad , \tag{16}$$

$$\Gamma_{B_s^0/\bar{B}_s^0 \to \bar{f}}(t) = 2 \cdot |\bar{A}_{\bar{f}}|^2 (1 + |\bar{\lambda}_{\bar{f}}|^2) \frac{e^{-\Gamma_s t}}{2} \cdot \left(\cosh \frac{\Delta\Gamma_s t}{2} + D_{\bar{f}} \sinh \frac{\Delta\Gamma_s t}{2} \right) \quad . \tag{17}$$

These equations demonstrate that in the case of a non-zero value of $\Delta\Gamma_s$ the decay rate distributions of the untagged samples are sensitive to the observables D_f and $D_{\bar{f}}$, which are proportional to $Re(\lambda_f)$ and $Re(\bar{\lambda}_{\bar{f}})$. In Fig. 8 we show an example of generated events and maximized likelihood of the two untagged decay flavours.

Similarly as in section 4.2 where only tagged events were included in the study, we performed 400 "experiments" and collected the information on the fitted parameters. We report the results from the $B_s^0 \to D_s^- \pi^+$ and $B_s^0 \to D_s^\mp K^\pm$ decay channels, when including untagged $B_s^0 \to D_s^\mp K^\pm$ events, in Tab. 4. The expected resolution on the weak and strong phases after 1 year of data taking improves by $\sim 2^\circ$ due to the inclusion of the untagged $B_s^0 \to D_s^\mp K^\pm$ events in the analysis. The sensitivity to Δm_s and ω remain unchanged, as expected.

Sensitivity results from $B_s^0 \to D_s^- \pi^+$ and $B_s^0 \to D_s^\mp K^\pm$ including untagged $B_s^0 \to D_s^\mp K^\pm$ events					
	$\Delta m_s\,(\mathrm{ps}^{-1})$	ω	$\lvert\lambda_f\rvert$	$\gamma + \phi_s\,(^\circ)$	$\Delta_{T1/T2}\,(^\circ)$
Input value	17.5	0.328	0.37	60	0
Fitted value	17.5	0.3279	0.372	60.4	0.5
σ (5y)	0.003	0.0013	0.027 ± 0.001	4.6 ± 0.17	4.6 ± 0.17
σ (1y)	0.007	0.0030	0.061	10.3	10.3

Table 4: Sensitivity results from $B_s^0 \to D_s^- \pi^+$ and $B_s^0 \to D_s^\mp K^\pm$, including untagged $B_s^0 \to D_s^\mp K^\pm$ events.

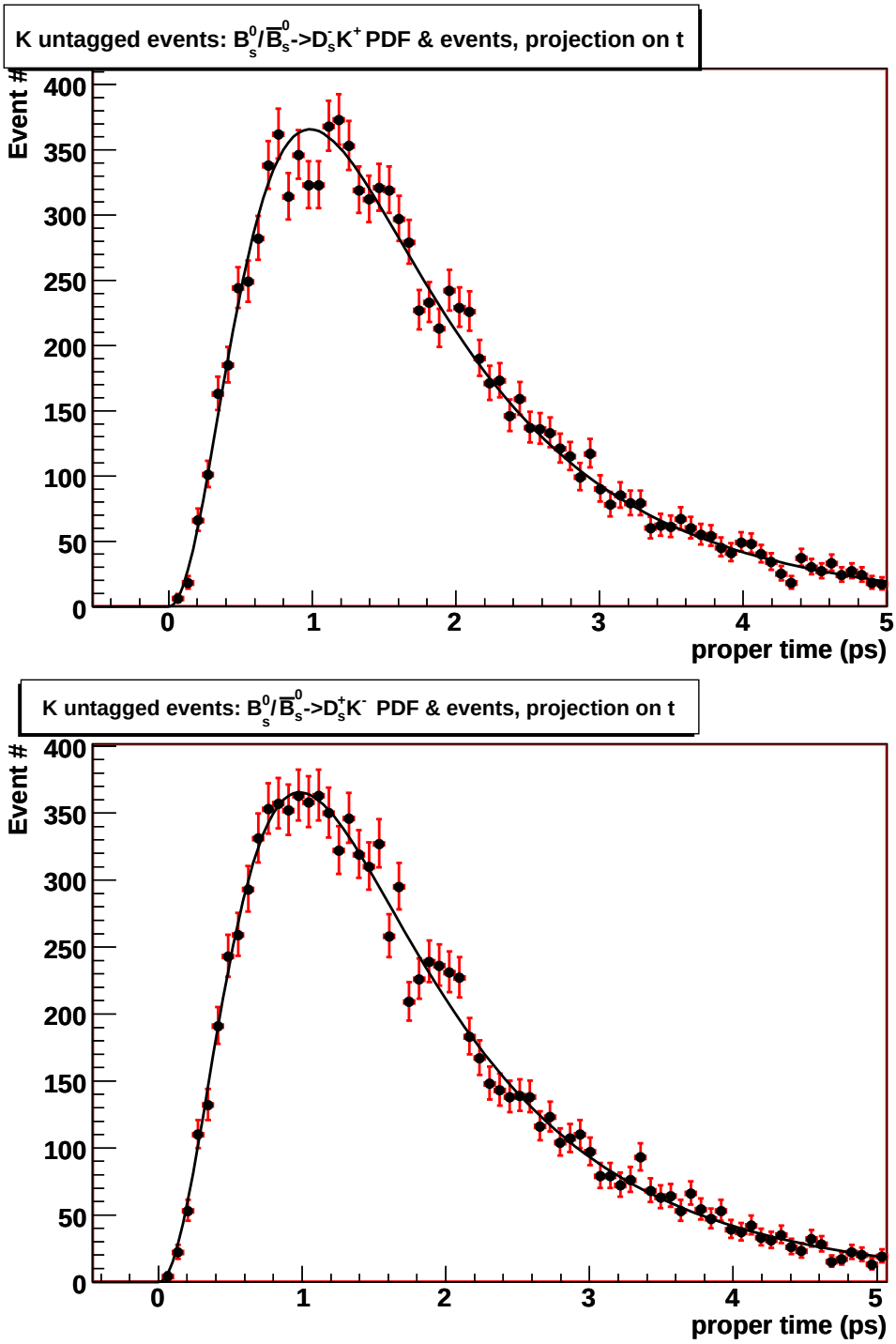

Figure 8: RooFit simulated events and maximized likelihood curve projected onto the proper time axis for the two untagged decay equations, $B_s^0/\bar{B}_s^0 \to D_s^- K^+$ (top) and $B_s^0/\bar{B}_s^0 \to D_s^+ K^-$ (bottom). The distributions represent 10 fb^{-1} of data.

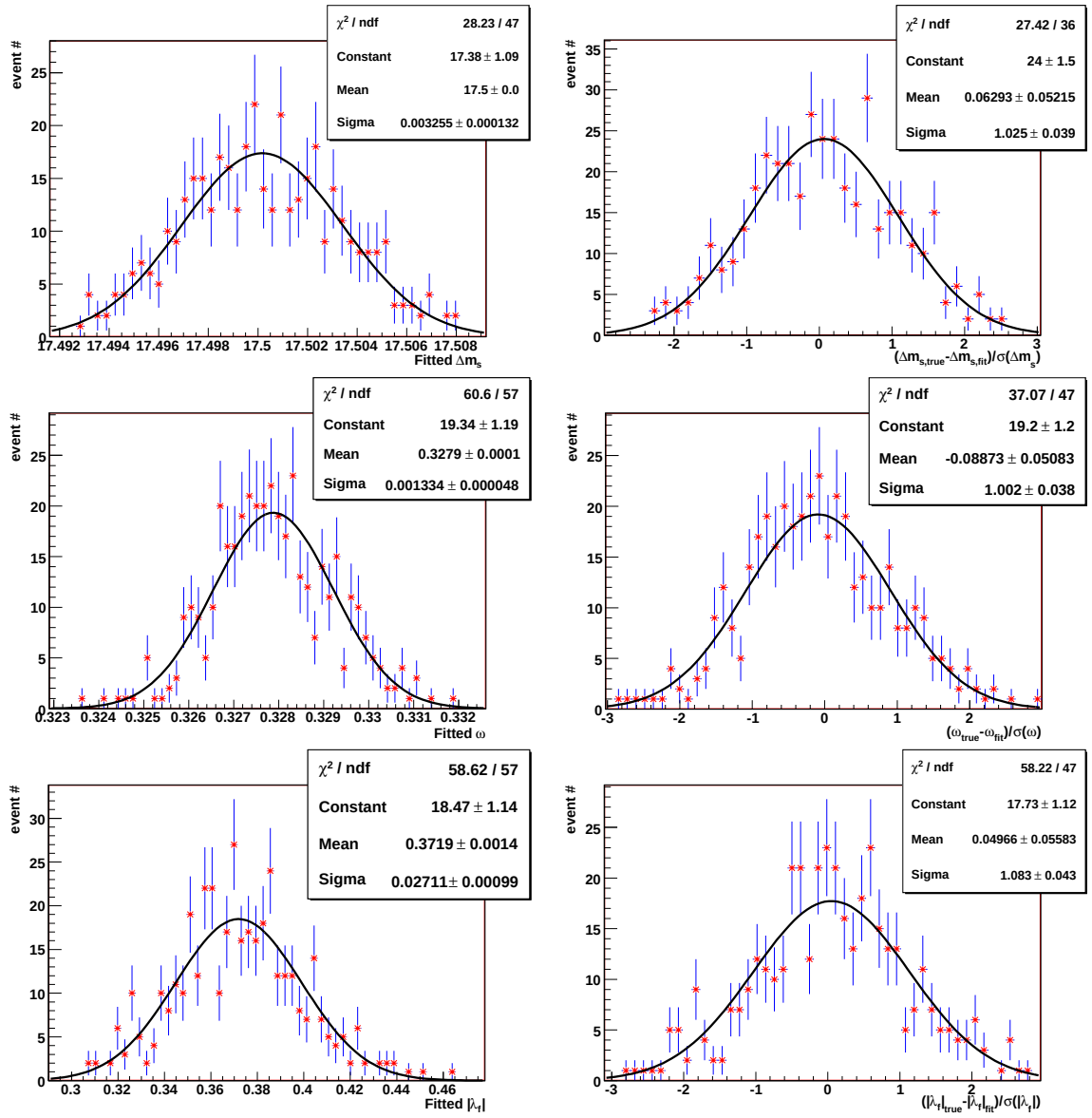

Figure 9: Fitted parameter values and pull distributions for the study including $B_s^0 \to D_s^{\mp} K^{\pm}$ untagged events: Δm_s fitted values distribution (top left) and pull distribution (top right), mistag rate ω fitted values (middle left) and pull (middle right) distributions, and $|\lambda_f|$ fitted values (bottom left) and pull (bottom right) distributions. Each distribution contains 400 entries.

Figs. 9 and 10 present plots of the fitted parameters and pull distributions. The results reported in Tab. 4 were obtained from these distributions. Each distribution was fitted with a Gaussian. The pull distributions all give good results with a pull mean consistent with 0 and a pull standard deviation consistent with 1.

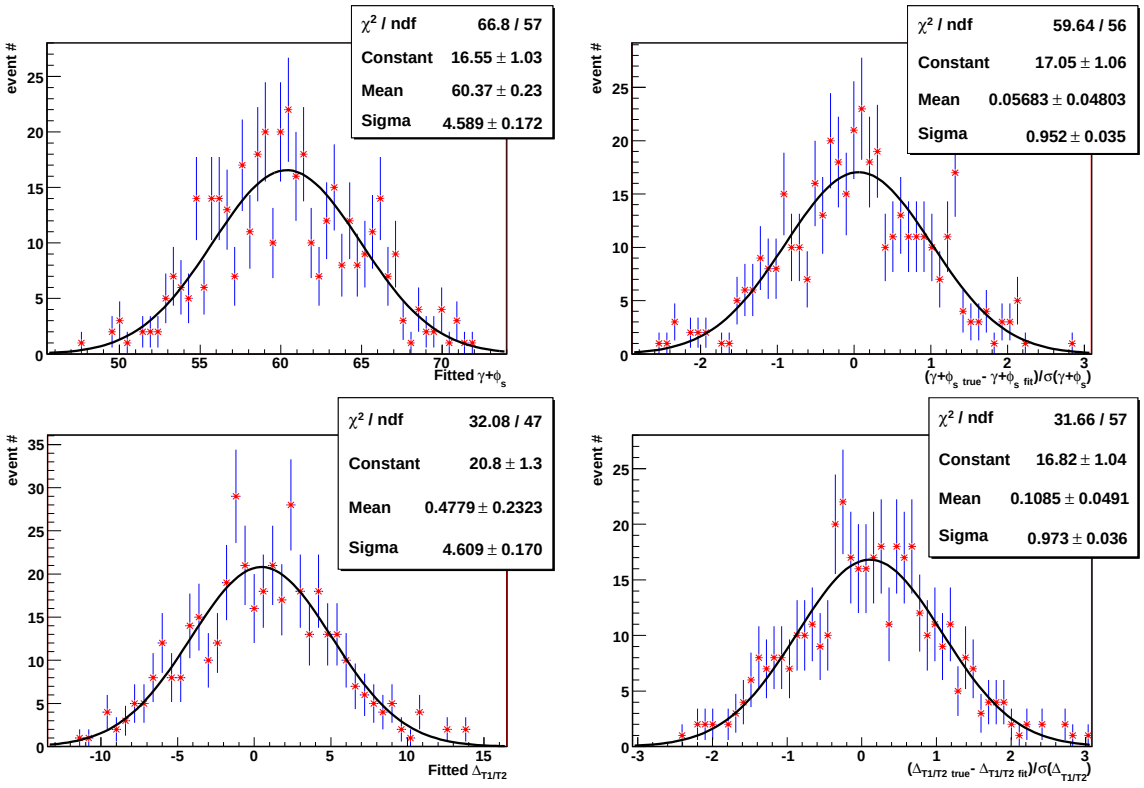

Figure 10: Fitted parameter values and pull distributions for the study including $B_s^0 \to D_s^{\mp} K^{\pm}$ untagged events: The weak phase, $\gamma + \phi_s$, fitted values distribution (top left) and pull distribution (top right), and the strong phase, $\Delta_{T1/T2}$, fitted values (bottom left) and pull (bottom right) distributions. Each distribution contains 400 entries. The pull distributions do not indicate any problems.

4.4 Results for different input values

Since the theoretical prediction on the strong phase $\Delta_{T1/T2}$ is not well determined and the expected experimental B/S ratio and mistag rate ω have large uncertainties, a systematic study was performed to see how the expected resolutions change if these parameters have different values from what was assumed so far. Similarly to above, we ran 400 "experiments", including the untagged $B_s^0 \to D_s^{\mp} K^{\pm}$, but with different input values for the strong phase, the B/S ratio for the $B_s^0 \to D_s^{\mp} K^{\pm}$ channels, and the mistag rate.

The summarized results of the systematic studies are reported in Tab. 5 for different strong phase input values, in Tab. 6 for different B/S ratios for the $B_s^0 \to D_s^{\mp} K^{\pm}$ channels, and in Tab. 7 for different ω input values. If not otherwise mentioned, the input value of the physics parameters remain as in section 4.3. Tables 5, 6 and 7 report the resolutions on the weak and the strong phases.

Results for different $\Delta_{T1/T2}$ values			
$\Delta_{T1/T2}\,(^\circ)$	-20	0	$+20$
$\sigma(\gamma+\phi_s)\,(^\circ)$	11.2	10.3	10.4
$\sigma(\Delta_{T1/T2})\,(^\circ)$	10.4	10.3	11.3

Table 5: Sensitivity results for different strong phase input values. Results are reported for one year of data taking.

Results for different $B_s^0 \to D_s^{\mp} K^{\pm}$ B/S values			
B/S	0.0	0.7	2.0
$\sigma(\gamma+\phi_s)\,(^\circ)$	9.6	10.3	11.1
$\sigma(\Delta_{T1/T2})\,(^\circ)$	10.9	10.3	11.6

Table 6: Sensitivity results for $B_s^0 \to D_s^{\mp} K^{\pm}$ different B/S values. Results are reported for one year of data taking.

In Tab. 5 we observe that the expected resolution on the weak phase deteriorates by $\sim 1^\circ$ if $\Delta_{T1/T2} = -20^\circ$, while it almost does not change if $\Delta_{T1/T2} = 20^\circ$.

In Tab. 6 we observe that the expected resolution on the weak phase would improve by $\sim 1^\circ$ if there were no background for the $B_s^0 \to D_s^{\mp} K^{\pm}$ channels. On the other hand, the expected resolution on the weak phase would deteriorate only by $\sim 1^\circ$ for a high level of background ($B/S = 2$) for the $B_s^0 \to D_s^{\mp} K^{\pm}$ channels.

The sensitivity on Δm_s, the mistag rate ω and $|\lambda_f|$ remain the same as in section 4.3 for both these "robustness" studies. The fitted values did not show any systematic shift.

Results for different ω values					
ω	0.29	0.31	0.328	0.35	0.37
$\sigma(\Delta m_s)\,(\mathrm{ps}^{-1})$	0.006	0.007	0.007	0.008	0.010
$\sigma(\lvert\lambda_f\rvert)$	0.049	0.054	0.061	0.066	0.069
$\sigma(\gamma+\phi_s)\,(^\circ)$	9.3	10.1	10.3	11.7	12.3
$\sigma(\Delta_{T1/T2})\,(^\circ)$	9.4	10.4	10.3	12.0	12.0

Table 7: Sensitivity results for different mistag rate input values. Results are reported for one year of data taking.

The dependence of the expected resolutions on the mistag rate ω is presented in Tab. 7 for a relatively large range. As expected, the resolutions improve with decreasing ω. Improving ω by $\sim 10\%$ (relative to the nominal 0.328 value) results in a 1° improved sensitivity on the weak and strong phases; likewise the sensitivity on Δm_s and $|\lambda_f|$ improves by about 10%.

4.5 Results with floating scale factor

A floating scale factor in the likelihood fit can be used to indicate whether the proper time errors are underestimated, correct or overestimated. For underestimated proper time errors the fitted scale factor will be larger than its input value, for correctly estimated proper time errors the scale factor fitted value should be equal to its input value and for overestimated proper time errors one would get a fitted scale factor smaller than its input value. When running with events from a real experiment such a check can be very useful, while in a MC study one expects to find a fitted scale factor corresponding to the input value. For all results presented hitherto the signal scale factor, S_{sig}, and the background scale factor, S_{bg}, that are included in the likelihood function (Eq. 13) remained fixed parameters in the fit.

The effect of a finite proper time resolution is to damp the B_s^0 oscillations. Such damping also arises from incorrect decisions in flavour tagging. Therefore determining both the signal scale factor for the proper time errors, S_{sig}, and the mistag fraction ω, relies on the measurement of the amplitude of the B_s^0 oscillations. Note that this is only true for the events in the $B_s^0 \to D_s^-\pi^+$ sample as the amplitudes of the observed oscillations in the $B_s^0 \to D_s^\mp K^\pm$ sample are affected by the CP asymmetry that is being fitted at the same time. Although the effect of wrong tag assignment and decay time smearing is a dampening of the oscillations, the net effect in a sample of reconstructed events can be different since the decay time resolution is *known for each event* via the track reconstruction and vertexing algorithms. Due to the fact that these assigned errors include a wide spectrum, as shown

Sensitivity results with floating signal scale factor S_{sig}						
	$\Delta m_s\,(\mathrm{ps}^{-1})$	ω	$\lvert\lambda_f\rvert$	$\gamma+\phi_s\,(^\circ)$	$\Delta_{T1/T2}\,(^\circ)$	S_{sig}
Input value	17.5	0.328	0.37	60	0	1.175
Fitted value	17.5	0.3278	0.372	60.3	0.4	1.176
σ (5y)	0.003	0.0028	0.026	4.7	4.6	0.045
σ (1y)	0.007	0.0063	0.058	10.5	10.4	0.100

Table 8: Sensitivity results with floating signal scale factor S_{sig}.

in Fig. 7, a sensitivity for each effect can be obtained.

In order to check if the signal scale factor and the mistag fraction can be determined simultaneously, we ran again 400 "experiments" where we have the following floating parameters: Δm_s, ω, $|\lambda_f|$, $arg(\lambda_f)$, $arg(\bar{\lambda}_{\bar{f}})$ and the signal scale factor S_{sig}. The background scale factor S_{bg} remains a fixed parameter in this study.

We find that the likelihood maximization converges for all experiments without any problems. We report the sensitivity results from this study in Tab. 8. (Unless otherwise mentioned, the input values of the different parameters are the same as in section 4.3. Untagged $B_s^0 \to D_s^{\mp} K^{\pm}$ events are included in the analysis.)

Comparing Tab. 8 to the results in section 4.3 (Tab. 4) we find that the resolutions on Δm_s, $|\lambda_f|$, $\gamma+\phi_s$ and $\Delta_{T1/T2}$ remain mainly unchanged. The one-year resolution on the mistag fraction ω has worsened by a factor two to $\sigma(\omega) = 0.006$ and the one-year resolution on the signal scale factor is around 10% of its input value.

The ω and S_{sig} fitted parameter values and pull distributions are presented in Fig. 11. For both parameters the pull distribution indicates underestimated errors as $\sigma(\mathrm{pull}) \approx 1.2$. The pull distributions for the other floating parameters do not indicate any problems.

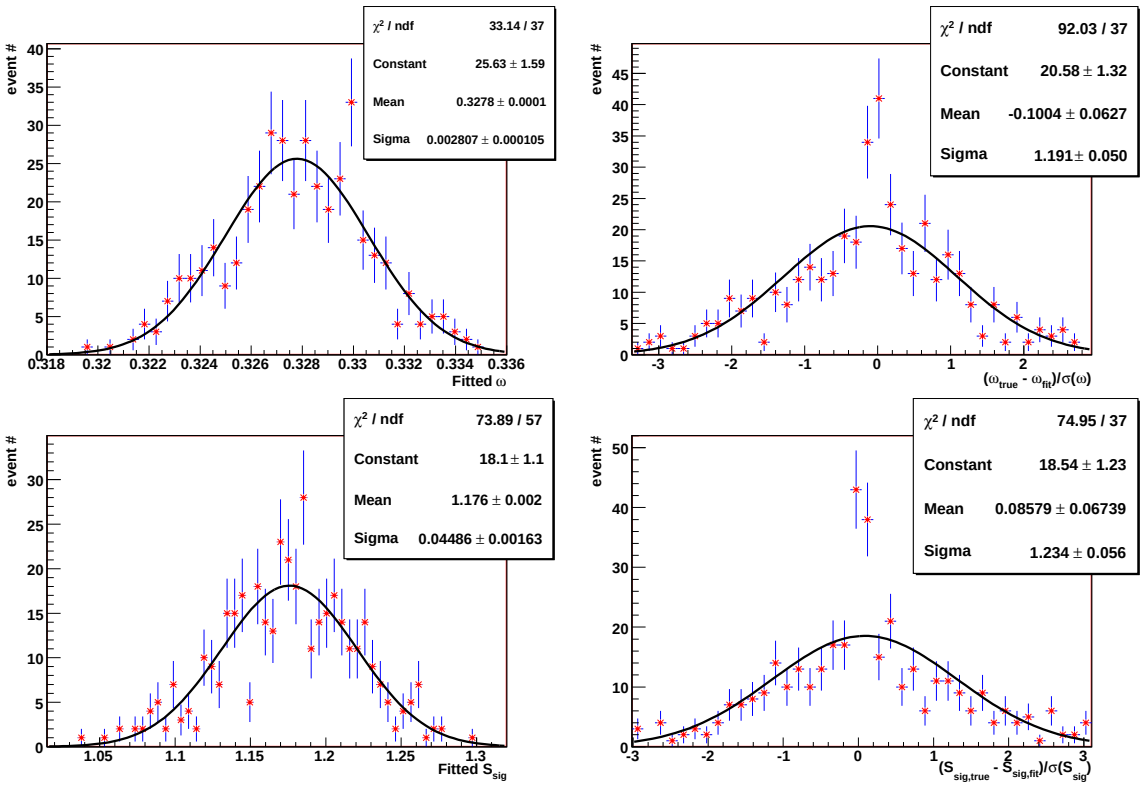

Figure 11: Fitted parameter values and pull distributions for the sensitivity study with a floating signal scale factor S_{sig}. Mistag fraction ω fitted values (top left) and pull (top right) distribution plots, signal scale factor S_{sig} fitted values (bottom left) and pull (bottom right) distribution plots. Each distribution contains 400 entries.

5 Summary

With the current toy Monte Carlo RooFit sensitivity studies for the decay channels $B_s^0 \to D_s^- \pi^+$ and $B_s^0 \to D_s^{\mp} K^{\pm}$ presented in this note, we report expected one-year sensitivities of $\sigma(\Delta m_s) = 0.007\,\mathrm{ps}^{-1}$, $\sigma(\omega) = 0.003$, $\sigma(\gamma + \phi_s) = 10.3^\circ$ and $\sigma(\Delta_{T1/T2}) = 10.3^\circ$ for nominal input values, when untagged $B_s^0 \to D_s^{\mp} K^{\pm}$ events are included in the study. We note an improvement of $\sim 2^\circ$ in the resolutions of $\gamma + \phi_s$ and $\Delta_{T1/T2}$ compared to a study where the untagged $B_s^0 \to D_s^{\mp} K^{\pm}$ events were not included.

Checking the effect of the $B_s^0 \to D_s^{\mp} K^{\pm}$ background level on the resolutions, we see that if there was no background to the $B_s^0 \to D_s^{\mp} K^{\pm}$ channel then the resolution on $\gamma + \phi_s$ would improve by $\sim 0.7^\circ$, while if there was high background level of $B/S = 2$ then the resolution would deteriorate by $\sim 0.8^\circ$.

The expected resolutions depend on the experimentally determined mistag faction ω – the resolutions on the weak and strong phases improve with decreasing ω. Improving ω by $\sim 10\%$ relative to the nominal $\omega = 0.328$ value results in a 1° improved sensitivity on the weak and strong phases.

We observe that the resolutions on the weak and strong phases deteriorate by a maximum of 1° if the strong phase value is -20° or $+20^\circ$ instead of the nominal 0°.

A further study proves that it is possible to determine the mistag fraction ω and the signal scale fraction S_{sig} simultaneously. The expected resolutions in such study are $\sigma(\omega) = 0.0063$ and $\sigma(S_{sig}) = 0.1$.

A Fit to the asymmetry observables

The analysis presented in this note can also be performed directly in terms of the asymmetry variables C_f, S_f, D_f, $S_{\bar{f}}$ and $D_{\bar{f}}$ (Eq. 9). According to Eqs. 5-8, a likelihood fit to these observables is a model-independent method. Information on the (LHCb) sensitivity to the asymmetry observables is valuable for other CP-violation studies: it has been shown in [9] and references therein how they can serve as input in other methods of extraction of γ. Both channels $B_s \to D_s^{\pm} K^{\mp}$ and $B_d \to D^{\pm}\pi^{\mp}$ are used in a combined analysis, under the assumption of U-spin symmetry, to reduce the number of ambiguous solutions for γ present in most methods.

In what follows we have repeated a toy MC study of 400 "experiments" using precisely the same input and physics parameters as in the study presented in section 4.2. Likewise, only tagged $B_s^0 \to D_s^- \pi^+$ and $B_s^0 \to D_s^{\mp} K^{\pm}$ events were considered.

The combined likelihood for $B_s^0 \to D_s^- \pi^+$ and $B_s^0 \to D_s^{\mp} K^{\pm}$ was simultaneously maximized, as before. The difference comes from the set of floating parameters in the fit, which are here: Δm_s, ω, C_f, S_f, D_f, $S_{\bar{f}}$ and $D_{\bar{f}}$. The input values of the asymmetry variables were calculated from the parameters in Tab. 2 and their definitions, Eq. 9.

Comparing with the fit of section 4.2, two extra floating parameters are introduced: the set ($|\lambda_f| (= |\bar{\lambda}_{\bar{f}}|)$, $arg(\lambda_f)$, $arg(\bar{\lambda}_{\bar{f}})$) becomes ($C_f$, S_f, D_f, $S_{\bar{f}}$ and $D_{\bar{f}}$). These extra degrees of freedom relate to the constraints not used in this study. Indeed, $C_f = C_{\bar{f}}$ under our assumptions (see section 2). Furthermore, it is straightforward to check from Eq. 9 that the asymmetry observables obey the constraints

$$C_f^2 + S_f^2 + D_f^2 = 1 \quad , \quad C_{\bar{f}}^2 + S_{\bar{f}}^2 + D_{\bar{f}}^2 = 1 \quad . \tag{18}$$

Sensitivity results from $B_s^0 \to D_s^- \pi^+$ and $B_s^0 \to D_s^{\mp} K^{\pm}$ without constraint on asymmetry observables							
	$\Delta m_s\,(\mathrm{ps}^{-1})$	ω	C_f	S_f	D_f	$S_{\bar{f}}$	$D_{\bar{f}}$
Input value	17.5	0.328	0.759	-0.564	0.325	0.564	0.325
Fitted value	17.5	0.328	0.760	-0.568	0.328	0.559	0.335
σ (5y)	0.003	0.0013	0.046	0.063	0.119	0.065	0.126
σ (1y)	0.007	0.003	0.104	0.141	0.267	0.144	0.282

Table 9: Sensitivity results on the asymmetry observables from $B_s^0 \to D_s^- \pi^+$ and $B_s^0 \to D_s^{\mp} K^{\pm}$ tagged event samples.

A.1 Fit without constraint

The results on the sensitivity to the asymmetry observables are presented in Tab. 9. The resolutions on Δm_s, ω are to be compared with those from Tab. 3; they are identical, as expected.

The asymmetry observables are correctly determined by the likelihood fit. One-year resolutions of the order of $10 - 30\%$ are achieved.

As the constraint Eq. 18 was not imposed during the fit, the distributions of $C_f^2+S_f^2+D_f^2$ and $C_{\bar{f}}^2 + S_{\bar{f}}^2 + D_{\bar{f}}^2$ may serve as a cross-check of the correctness of the final fit results. Both were found to follow a Gaussian distribution centered around 1.

All fit parameters pull distributions are unbiased and consistent with a unit width, showing a correct estimation of the fit errors. The asymmetry observables possess (global) correlations of typically 0.2.

Sensitivity results from $B_s^0 \to D_s^- \pi^+$ and $B_s^0 \to D_s^\mp K^\pm$ with constraint on asymmetry observables					
	$\Delta m_s\,(\mathrm{ps}^{-1})$	ω	C_f	S_f	$S_{\bar{f}}$
Input value	17.5	0.328	0.759	-0.564	0.564
Fitted value	17.5	0.328	0.754	-0.561	0.565
σ (5y)	0.003	0.0013	0.031	0.049	0.045
σ (1y)	0.007	0.003	0.070	0.110	0.101

Table 10: Sensitivity results on the asymmetry observables from $B_s^0 \to D_s^- \pi^+$ and $B_s^0 \to D_s^\mp K^\pm$ tagged event samples. The constraints Eq. 18 were used to "remove" D_f and $D_{\bar{f}}$ from the fit.

A.2 Fit with constraint

We have repeated the same study as above but imposing the two constraints on D_f and $D_{\bar{f}}$ (Eq. 18), reducing the set of fit floating parameters to Δm_s, ω, C_f, S_f and $S_{\bar{f}}$ (D_f and $D_{\bar{f}}$ are "removed" from the fit).

Table 10 presents the sensitivities on the fitted parameters. The one-year resolutions on C_f, S_f and $S_{\bar{f}}$ improve by as much as $20 - 30\%$ compared to the resolutions from the non-constrained fit.

The sensitivity on the D_f and $D_{\bar{f}}$ observables can be extracted from the constraints: we obtain in both cases a Gaussian distribution (from the 400 "experiments") centered around

the correct value and with a five-year resolution of about 0.8, *i.e.* 30% better than obtained with the "non-constrained fit".

All pull distributions are unbiased and consistent with a unit width. The asymmetry observables are in this case rather correlated, with mean (global) correlations of typically $0.5 - 0.6$. The mean correlation between C_f and S_f ($S_{\bar{f}}$) and S_f and $S_{\bar{f}}$ are ≈ 0.3 and 0.5, respectively.

References

[1] W. Verkerke and D. Kirkby, "The RooFit toolkit for data modeling", Proceedings of Computing in High Energy and Nuclear Physics (CHEP03), La Jolla, Ca. USA, March 2003, arXiv:physics/0306116

[2] J. Borel et al., "The $B_s^0 \to D_s^- \pi^+$ and $B_s^0 \to D_s^\mp K^\pm$ selections.", LHCb-2007-017.

[3] G. Raven, "Sensitivity Studies of χ and $\Delta\Gamma$ with $B_s \to J/\psi(\mu^+\mu^-)\phi(K^+K^-)$", LHCb-2003-119.

[4] P. Vankov, "Sensitivity to the B_s^0 mixing phase at LHCb", LHCb-2007-065.

[5] M. Calvi et al., "Flavour tagging algorithms and performances in LHCb.", LHCb-2007-058.

[6] F. James, "MINUIT minimization package", Reference Manual, Version 94.1, 1994, CERN/PACKLIB software library

[7] R. Hierck, J. van Hunen and M. Merk, "The sensitivity for Δm_s and $\gamma + \phi_s$ from $B_s^0 \to D_s^- \pi^+$ and $B_s^0 \to D_s^\mp K^\pm$ decays.", LHCb-2003-103.

[8] J. van Tilburg, "Track simulation and reconstruction in LHCb.", Ph.D. thesis, NIKHEF 2005, CERN-THESIS/2005-040.

[9] G. Wilkinson, "Extraction of γ at LHCb with a Combined $B_s \to D_s^\pm K^\mp$ and $B_d \to D^\pm \pi^\mp$ Analysis, LHCb-2005-036.